Robotica (2024), **42**, pp. 1549–1567
doi:10.1017/S0263574724000365

CAMBRIDGE UNIVERSITY PRESS

RESEARCH ARTICLE

Inverse dynamics analysis of a 6-RR-RP-RR parallel manipulator with offset universal joints

Huze Huang[1,2], Hasiaoqier Han[1,3], Dawei Li[1], Zhenbang Xu[1,3] and Qingwen Wu[1,3]

[1]Changchun Institute of Optics, Fine Mechanics and Physics, Chinese Academy of Sciences, Changchun, China, [2]University of Chinese Academy of Sciences, Beijing, China, and [3]Center of Materials Science and Optoelectronics Engineering, University of Chinese Academy of Sciences, Beijing, China
Corresponding author: Hasiaoqier Han; Email: hanhasiaoqier@yahoo.com

Received: 10 May 2023; **Revised:** 27 January 2024; **Accepted:** 19 February 2024; **First published online:** 26 March 2024

Keywords: parallel manipulator; precision adjustment platform; robot dynamics; offset universal joint; Newton–Euler method; GMRES

Abstract

This paper presents an algorithm for solving the inverse dynamics of a parallel manipulator (PM) with offset universal joints (RR–joints) via the Newton–Euler method. The PM with RR–joints increase the joint stiffness and enlarge the workspace but introduces additional joint parameters and constraint torques, rendering the dynamics more complex. Unlike existing studies on PMs with RR–joints, which emphasize the kinematics and joint performance, this paper studies the dynamical model. First, an iterative algorithm is established through a rigid body velocity transformation, which calculates the input parameters of the link velocity and acceleration. A linear system of equations in matrix form is then established for the entire PM through the Newton–Euler method. By using the generalized minimal residual method (GMRES) to solve the equation system, all the forces and torques on the joints can be obtained, from which the required actuation force can be derived. This method is validated through numerical simulations using the automatic dynamic analysis of multibody systems software. The proposed method is suitable for establishing the dynamic model of complex PMs with redundant or hybrid structures.

1. Introduction

The first successfully applied parallel manipulator (PM) structure was originally developed by Gough and later modified by Stewart [1, 2]. Over the past two decades, the research direction and application of PMs has shifted toward control, coordination, and algorithms, rather than emphasizing the development of new structures. This places additional demands on the study of the PM dynamics.

To achieve higher performance requirements, we propose a new 6-RR-RP-RR configuration, where P, R, and RP denote prismatic, revolute joints, and an actuated ball screw assembly, respectively. Compared with the Stewart platform, the dynamics of PMs with RR–joints are complicated by the additional torques. Nevertheless, a study by Gloess and Lula [3] on the impact of the RR–joint on the stiffness of a PM found that it provides twice the joint stiffness of a conventional universal joint. Additionally, the axial rotation range was extended to $\pm 90^{\circ}$ in both joint shifts, thereby expanding the workspace of the PM [4]. More importantly, in the application process, we have realized that the offset RR–joint, compared to the conventional universal joint, can divide the joint into several parts, significantly reducing the manufacturing complexity of the joint. Moreover, during the installation process, it provides more installation space, making it more suitable for PM designed for mass production purposes. In conclusion, it is meaningful to consider the dynamics of PMs with RR–joints.

In recent years, there has been a rapid increase in theoretical research on PMs with RR–joints, particularly the computation of their kinematics. Analysis of the workspace of a 3-RR-P-RR PM [5] showed that it has a larger reachable workspace than similar structures using only one RR–joint or none at all.

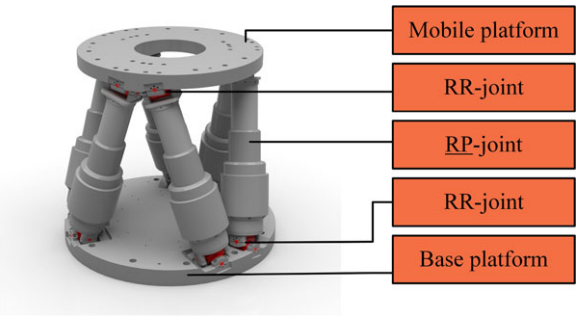

Figure 1. *The CAD model of the 6-RR-RP-RR PM.*

Algorithms based on joint constraints [6, 7] have attempted to establish the displacement kinematics of a 6-RR-C-RR PM with RR–joints (where C denotes a cylindrical joint whose translational degree of freedom (DOF) is actuated). Additionally, the displacement kinematics of a 6-P-RR-R-RR PM have been studied using both the joint-constraint algorithm and the Denavit–Hartenberg (D–H) parameters [8, 9], with numerical solutions obtained. The displacement kinematics of a 6-RR-RP-RR PM (see Fig. 1) was analyzed by Yu et al. [10], while Zhang et al. [11] derived the velocity and acceleration solution of the PM by introducing the differential form of the kinematic model using the Jacobian matrix. To date, all research on PMs with RR–joints has focused on kinematics, rather than dynamics. The dynamic model of the 6-RR-RP-RR PM will be derived in this paper.

Several approaches have been developed for studying the dynamics of PMs, such as the principle of virtual work [12–14], Kane's method [15–17], Hamilton's principle [18], and screw theory [19–21]. Other common approaches include Lagrangian methods [22–24], Newton–Euler methods [25, 26], and hybrid techniques [27–29]. The Lagrangian method describes a system's motion from the energy perspective [30]. Therefore, there is no need to consider the internal force or changes in the reference frame system [31]. In contrast, the Newton–Euler method is more efficient but requires the internal forces of links to be considered [32]. The motion of links in space has six degrees-of-freedom (DOFs). The Newton equation and the Euler equation provide the constraint equations for translational and rotational movements, respectively.

As an efficient and convenient approach, the Newton–Euler method has been widely used in recent years. For instance, Chen and Wang [33] used this method to establish a dynamic model for a redundantly actuated cable-driven PM, while Arian et al. [34] employed the Newton–Euler method to model the dynamics of a 3-DOF Gantry–Tau manipulator. The legs of a PM can be considered as a series mechanism, allowing for the development of an efficient iterative dynamic model through the iteration of both outward motion and inward forces. Importantly, the effect of the mobile platform at the end of the legs must be taken into consideration. In this way, He et al. [35] applied the Newton–Euler method to obtain a dynamic model for a 7-DOF hybrid serial–parallel manipulator.

By applying the Newton–Euler approach, this article presents a dynamic algorithm for a 6-RR-RP-RR PM. First, we develop an iterative algorithm for determining the relationship between joint motion and link motion. Next, we establish a dynamic model using the Newton–Euler equations and a linear equation system. We then analyze the actuated forces, before validating the accuracy of the mathematical model through simulations.

The remainder of this paper is organized as follows. Section 2 describes the manipulator and the definition of the joints' reference frame. Section 3 describes the inverse kinematic model of the PM joints and then proposes an iterative algorithm for computing the link motion in the base frame. Section 4 establishes the dynamic model of the PM using the Newton–Euler method and solves the equation system with a sparse coefficient matrix by generalized minimal residual method (GMRES). Section 5 solves the dynamic model and compares it with the simulation model. Finally, Section 6 presents the conclusions to this study.

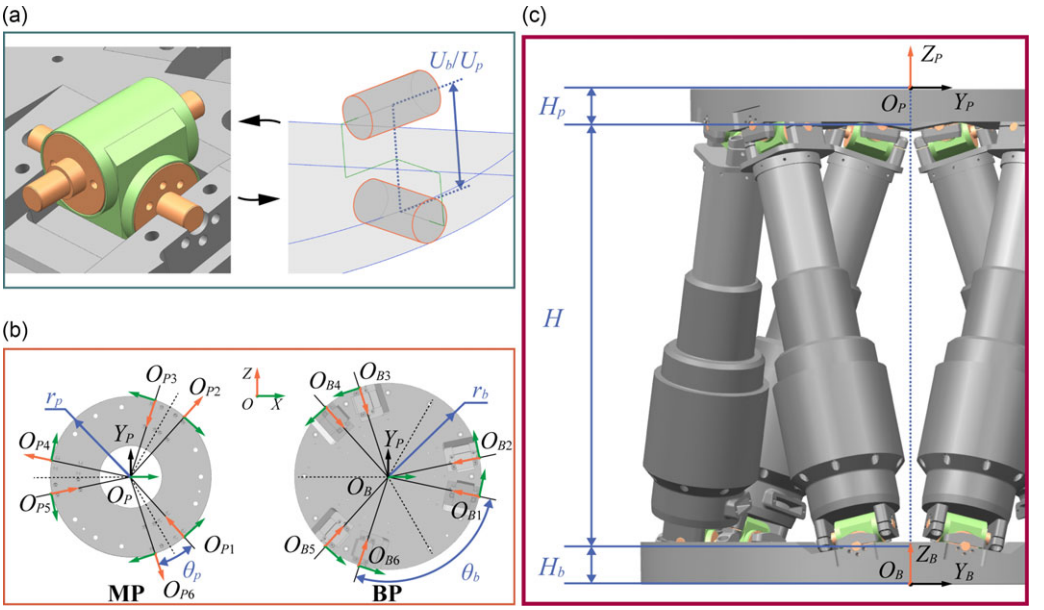

Figure 2. *Configuration, geometric parameters, and frame definition: (a) simplified form of the RR–joint and the offset value; (b) frame definition for MP and BP; (c) y-axis and z-axis of the frames $\mathcal{P}$ and $\mathcal{B}$, and geometric parameters in the axial direction.*

2. Manipulator description

The 6-RR-RP-RR PM studied in this paper consists of a mobile platform (MP), a base platform (BP), and six actuated legs which consist of a RP–joint and two RR–joints, as shown in Fig. 1.

Fig. 2 shows the configuration, geometric parameters, and the frames of the PM. Fig. 2a shows the used RR–joints and their simplified form. U_p and U_b are the offset values of the RR–joints on the MP and BP sides, respectively. Fig. 2b defines the frames of the MP and BP, where the reference frame $O_P - X_P Y_P Z_P$ (the $\mathcal{P}$ frame) is centered on point O_P in the MP and the base frame $O_B - X_B Y_B Z_B$ (the $\mathcal{B}$ frame) is centered on O_B in the BP. The points at which the legs connect with the MP and BP are defined as $O_{Pj}(j = 1 \sim 6)$ and $O_{Bj}(j = 1 \sim 6)$, respectively. Additionally, the frames of the connecting points are defined as $\mathcal{P}_j$ and $\mathcal{B}_j$ and are transformed from the frames $\mathcal{P}$ and $\mathcal{B}$ through a specified transformation [11]. Fig. 2c shows another view of the frames $\mathcal{P}$ and $\mathcal{B}$, as well as the geometric parameters along the z-axis.

A single leg can be considered as a serial kinematic chain, and its reference frames can be determined using the D–H parameter method. As depicted in Fig. 3, the following frames and parameters can be defined: $O_{ij} - X_{ij} Y_{ij} Z_{ij}$ (denoted as frame $\mathcal{F}_{ij}$, where $i = 1 \sim 6$ and $j = 1 \sim 6$) represents the reference frame of the ith joint of the jth leg. Note that $\mathcal{F}_{6j}$ is equivalent to $\mathcal{P}_j$. The generalized motion parameters of the joints are denoted by:

$$\mathbf{q}_{ij} = \left[\theta_{1j}\ \theta_{2j}\ \theta_{3j}\ d_{4j}\ \theta_{5j}\ \theta_{6j}\right]^{\mathrm{T}},$$

θ_{ij} represent the rotational angle, and d_{ij} represents the distance of movement, which lie along the z-axis of their respective joint reference frames, with the subscript ij referring to the ith joint of the jth leg:

$$\mathbf{T}_i = \mathbf{Rot}\,(X, \alpha_i) \cdot \mathbf{Tran}\,(X, a_i) \cdot \mathbf{Rot}\,(Z, \theta_i) \cdot \mathbf{Tran}\,(Z, d_i) \tag{1}$$

where $\mathbf{T}_i$ is a homogeneous transformation matrix. $\mathbf{Rot}\,(X, \alpha_i)$ and $\mathbf{Rot}\,(Z, \theta_i)$ represent rotation about the x-axis and z-axis, respectively. $\mathbf{Tran}\,(X, a_i)$ and $\mathbf{Tran}\,(Z, d_i)$ represent translation along the x-axis and z-axis by a specified distance.

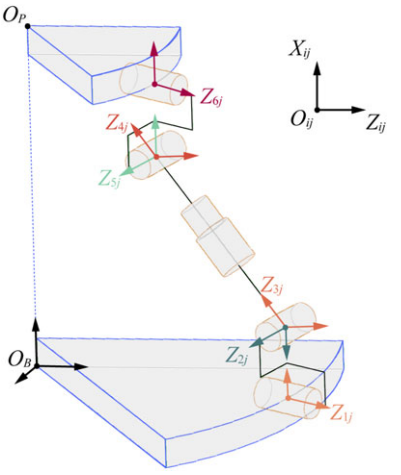

Figure 3. *Schematic of a single leg motion and distribution of joint frames. (The black frame in the top right corner represents the directional legend of the joint frames.).*

3. Kinematics

The inverse kinematic problem aims to uncover the connection between the position of the MP and the motion of each joint. Further, to establish the differential motion, including velocity and acceleration, the relationship between the MP and each leg is precisely defined through the Jacobian equations.

3.1. Inverse kinematic model

1. Displacement model: Due to the introduction of offset universal joints, a single leg is now regarded as a serial kinematic chain, resulting in the existence of multiple solutions for its inverse kinematic problem. Consequently, obtaining an explicit solution for the leg length is not straightforward through the geometric methods typically employed to solve the inverse kinematic problem of the Gough–Stewart Platform. Therefore, this paper solves the inverse displacement-kinematic problem of the PM using a numerical method [8]. Specifically, by obtaining a set of nonlinear equations with six unknowns through two equivalent homogeneous transformation matrices and solving the equations using the Newton–Raphson method, we obtain

$$\left[\mathbf{q}_{ij}\right]_{(k+1)} = \left[\mathbf{q}_{ij}\right]_{(k)} - \left[\frac{\partial \mathbf{\Phi}}{\partial \mathbf{q}_{ij}}\right]_{(k)}^{-1} \cdot \left[\mathbf{q}_{ij}\right]_{(k)} \tag{2}$$

with k represents the number of iterations. The nonlinear system consisting of six equations selected from the equivalent transformation is represented by $\mathbf{\Phi}$. And $[\mathbf{q}_{ij}]_{(0)}$ is the joint parameters of the current leg at the initial position. Detailed information on the above equation can be found in Appendix.

2. Velocity and acceleration models: The mapping matrix can be used to describe the velocity mapping relation between the MP and the joints [11]:

$$\dot{\mathbf{q}}_{ij} = \mathbf{J}_j^{-1} \cdot \dot{\mathbf{q}}_{MP}, \quad \mathbf{J}_j \in \mathbb{R}^{6\times 6} \tag{3}$$

and $\mathbf{J}_j$ can be decomposed into two parts:

$$\mathbf{J}_j = {}^{\dot{\mathbf{q}}_t}\mathbf{J}_{\dot{\mathbf{q}}_{MP}}^{-1} \cdot {}^{\dot{\mathbf{q}}_h}\mathbf{J}_{\dot{\mathbf{q}}_t}^{-1} \cdot {}^{\dot{\mathbf{q}}_h}\mathbf{J}_{\dot{\mathbf{q}}_{ij}} = {}^{\dot{\mathbf{q}}_h}\mathbf{J}_{\dot{\mathbf{q}}_{MP}}^{-1} \cdot {}^{\dot{\mathbf{q}}_h}\mathbf{J}_{\dot{\mathbf{q}}_{ij}} \tag{4}$$

where

$$^{\dot{\mathbf{q}}_h}\mathbf{J}_{\dot{\mathbf{q}}_{MP}} = {}^{\dot{\mathbf{q}}_h}\mathbf{J}_{\dot{\mathbf{q}}_t} \cdot {}^{\dot{\mathbf{q}}_t}\mathbf{J}_{\dot{\mathbf{q}}_{MP}}$$

relates to the motion of the MP. $^{\dot{\mathbf{q}}_h}\mathbf{J}_{\dot{\mathbf{q}}_t}$ is obtained by treating MP as a rigid body and analyzing the velocity transformation on the rigid body. $^{\dot{\mathbf{q}}_t}\mathbf{J}_{\dot{\mathbf{q}}_{MP}}$ is obtained by transforming Euler angular velocity to Cartesian angular velocity. And $^{\dot{\mathbf{q}}_h}\mathbf{J}_{\dot{\mathbf{q}}_{ij}}$ is the geometric Jacobian matrix which relates to the motion of the joints. The term $\dot{\mathbf{q}}_{ij} = \begin{bmatrix} \dot{\theta}_{1j} & \dot{\theta}_{2j} & \dot{\theta}_{3j} & \dot{d}_{4j} & \dot{\theta}_{5j} & \dot{\theta}_{6j} \end{bmatrix}^{\mathrm{T}}$ is the differential motion of joints, $\dot{\mathbf{q}}_{MP} = \begin{bmatrix} \dot{p}_x & \dot{p}_y & \dot{p}_z & \dot{\varphi} & \dot{\theta} & \dot{\psi} \end{bmatrix}^{\mathrm{T}}$ represents the first derivative of MP motion with respect to Euler angles by the sequence of RPY (Roll-Pitch-Yaw), $\dot{\mathbf{q}}_t = \begin{bmatrix} \dot{p}_x & \dot{p}_y & \dot{p}_z & \omega_x & \omega_y & \omega_z \end{bmatrix}^{\mathrm{T}}$ refers to the differential motion of the MP with respect to $\mathcal{B}$, and $\dot{\mathbf{q}}_h$ represents the differential motion of the point O_{Pj} in $\mathcal{B}$. Taking the time derivative of both sides of Eq. (3), the generalized acceleration of the leg joints is

$$\ddot{\mathbf{q}}_{ij} = \dot{\mathbf{J}}_j^{-1} \cdot \dot{\mathbf{q}}_{MP} + \mathbf{J}_j^{-1} \cdot \ddot{\mathbf{q}}_{MP} \tag{5}$$

with $\ddot{\mathbf{q}}_{MP}$ is the generalized acceleration of the MP concerning the Euler angle and $\ddot{\mathbf{q}}_{ij}$ is the joint acceleration.

3.2. Motion parameters of the MP

The MP can be considered as a parallel link, and the input velocity of O_P can be used to determine the motion parameters of the platform. Eq. (4) establishes the mapping relation between the generalized velocity of the MP $\dot{\mathbf{p}}_t$ in the frame $\mathcal{B}$ and its velocity $\dot{\mathbf{p}}_{MP}$ concerning the Euler angle. Thus, we obtain the generalized velocity of the MP as:

$$\dot{\mathbf{q}}_t = {}^{\dot{\mathbf{q}}_t}\mathbf{J}_{\dot{\mathbf{q}}_{MP}} \cdot \dot{\mathbf{q}}_{MP} = \begin{bmatrix} \dot{p}_x & \dot{p}_y & \dot{p}_z & \omega_x & \omega_y & \omega_z \end{bmatrix}^{\mathrm{T}} \tag{6}$$

Taking the time derivative of both sides of Eq. (6), the generalized acceleration of the MP is derived as:

$$\ddot{\mathbf{q}}_t = {}^{\dot{\mathbf{q}}_t}\dot{\mathbf{J}}_{\dot{\mathbf{q}}_{MP}} \cdot \dot{\mathbf{q}}_{MP} + {}^{\dot{\mathbf{q}}_t}\mathbf{J}_{\dot{\mathbf{q}}_{MP}} \cdot \ddot{\mathbf{q}}_{MP} = \begin{bmatrix} \ddot{p}_x & \ddot{p}_y & \ddot{p}_z & \dot{\omega}_x & \dot{\omega}_y & \dot{\omega}_z \end{bmatrix}^{\mathrm{T}} \tag{7}$$

with the angular velocity of the MP is $\boldsymbol{\omega}_{MP} = \begin{bmatrix} \omega_x & \omega_y & \omega_z \end{bmatrix}^{\mathrm{T}}$, the angular acceleration is $\dot{\boldsymbol{\omega}}_{MP} = \begin{bmatrix} \dot{\omega}_x & \dot{\omega}_y & \dot{\omega}_z \end{bmatrix}^{\mathrm{T}}$, and the acceleration is $\ddot{\mathbf{p}}_{MP} = \begin{bmatrix} \ddot{p}_x & \ddot{p}_y & \ddot{p}_z \end{bmatrix}^{\mathrm{T}}$.

In summary, the acceleration of the mass center of the MP under the frame $\mathcal{B}$ is given by:

$$\ddot{\mathbf{p}}_{CMP} = \ddot{\mathbf{p}}_{MP} + \dot{\boldsymbol{\omega}}_{MP} \times \mathbf{r}_{OP,CMP} + \boldsymbol{\omega}_{MP} \times \left(\boldsymbol{\omega}_{MP} \times \mathbf{r}_{OP,CMP} \right) \tag{8}$$

with $\mathbf{r}_{OP,CMP}$ is the vector from O_P to the mass center of the MP under the frame $\mathcal{B}$.

3.3. Iterative algorithm for velocity and acceleration of links

The motion parameters of the joints can be obtained from the inverse kinematic model. However, these parameters are all related to the z-axis of the joint frame $\mathcal{F}_{ij}$. To use the velocity and acceleration parameters as inputs for the dynamic model, they need to be transformed into the motion of the joint and link coordinate systems with respect to the base frame. To address this issue, an iterative algorithm is proposed for converting the joint motion.

The connection of adjacent joints is defined as a link, and the dynamic model requires the motion of these links as its input. Thus, an iterative algorithm (different from the previous Newton–Raphson iterative algorithm for the displacement kinematics) is adopted to obtain the motion parameters of each link under the frame $\mathcal{B}$.

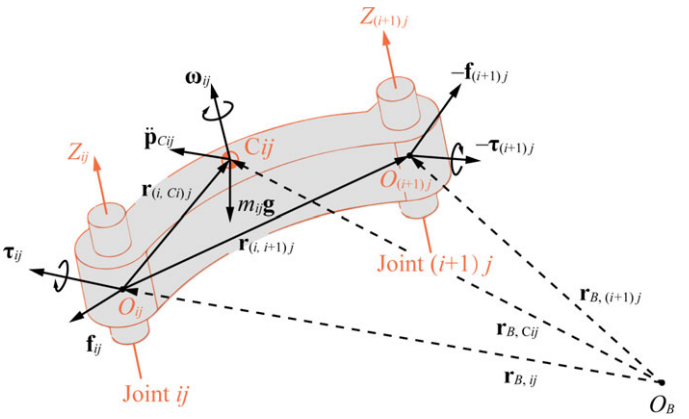

Figure 4. *Characterization of link L_{ij} for the Newton–Euler formulation.*

Any link L_{ij} can be represented as follows:

From Fig. 4, the parameters characterizing the motion of the link can be defined (see Table I).

The relationship between the motion of link L_{ij} and its joints is established through the following velocity transformation relation of the rigid body:

$$\boldsymbol{\omega}_{ij} = \begin{cases} \boldsymbol{\omega}_{(i-1)j} & \text{(P-joint)} \\ \boldsymbol{\omega}_{(i-1)j} + \dot{\theta}_{ij}\mathbf{Z}_{ij} & \text{(R-joint)} \end{cases} \tag{9}$$

and

$$\dot{\mathbf{p}}_{ij} = \begin{cases} \dot{\mathbf{p}}_{(i-1)j} + \dot{d}_{ij}\mathbf{Z}_{ij} + \boldsymbol{\omega}_{(i-1)j} \times \mathbf{r}_{(i-1,i)j} & \text{(P-joint)} \\ \dot{\mathbf{p}}_{(i-1)j} + \boldsymbol{\omega}_{(i-1)j} \times \mathbf{r}_{(i-1,i)j} & \text{(R-joint)} \end{cases} \tag{10}$$

By differentiating Eqs. (9) and (10), we obtain

$$\dot{\boldsymbol{\omega}}_{ij} = \begin{cases} \dot{\boldsymbol{\omega}}_{(i-1)j} & \text{(P-joint)} \\ \dot{\boldsymbol{\omega}}_{(i-1)j} + \ddot{\theta}_{ij}\mathbf{Z}_{ij} + \dot{\theta}_{ij}\left(\boldsymbol{\omega}_{ij} \times \mathbf{Z}_{ij}\right) & \text{(R-joint)} \end{cases} \tag{11}$$

and

$$\ddot{\mathbf{p}}_{ij} = \begin{cases} \ddot{\mathbf{p}}_{(i-1)j} + \ddot{d}_{ij}\mathbf{Z}_{ij} + 2\dot{d}_{ij}\left(\boldsymbol{\omega}_{(i-1)j} \times \mathbf{Z}_{ij}\right) \\ \quad + \dot{\boldsymbol{\omega}}_{(i-1)j} \times \mathbf{r}_{(i-1,i)j} + \boldsymbol{\omega}_{(i-1)j} \times \left(\boldsymbol{\omega}_{(i-1)j} \times \mathbf{r}_{(i-1,i)j}\right) & \text{(P-joint)} \\ \ddot{\mathbf{p}}_{(i-1)j} + \dot{\boldsymbol{\omega}}_{(i-1)j} \times \mathbf{r}_{(i-1,i)j} + \boldsymbol{\omega}_{(i-1)j} \times \left(\boldsymbol{\omega}_{(i-1)j} \times \mathbf{r}_{(i-1,i)j}\right) & \text{(R-joint)} \end{cases} \tag{12}$$

According to Eqs. (9), (11), and (12), and the geometry of the links, the acceleration of the mass center of link L_{ij} under the frame $\mathcal{B}$ can be determined as:

$$\ddot{\mathbf{p}}_{Cij} = \ddot{\mathbf{p}}_{ij} + \dot{\boldsymbol{\omega}}_{ij} \times \mathbf{r}_{(i,Ci)j} + \boldsymbol{\omega}_{ij} \times \left(\boldsymbol{\omega}_{ij} \times \mathbf{r}_{(i,Ci)j}\right) \tag{13}$$

As shown in Fig. 5, applying Eqs. (9), (11), and (13), the motion parameters for the links of the legs can be expressed in the frame $\mathcal{B}$. Here, $\boldsymbol{\omega}_{\mathcal{B}j}$, $\dot{\boldsymbol{\omega}}_{\mathcal{B}j}$, and $\ddot{\mathbf{p}}_{\mathcal{B}j}$ are the initial iterative parameters, determined by the motion of the BP. When the BP is stationary, these parameters are typically set to zeros.

4. Dynamics

With the use of RR–joints, both ends of the leg are affected by torques, the direction, and magnitude of which are unknown. Thus, the dynamic equation of the leg cannot be obtained explicitly. However, all forces and torques in the Newton–Euler method are linear and can be solved by establishing a system of linear equations.

Table I. *Variables of link L_{ij}.*

Variable	Value
m_{ij}	Mass of the L_{ij}
$\boldsymbol{\omega}_{ij}$, $\dot{\boldsymbol{\omega}}_{ij}$	Angular velocity and acceleration of L_{ij}
$\dot{\mathbf{p}}_{ij}$, $\ddot{\mathbf{p}}_{ij}$	Linear velocity and acceleration of O_{ij}
$\ddot{\mathbf{p}}_{Ci}$	Linear acceleration of the mass center C_{ij}
$\mathbf{f}_{ij}$	Force exerted by $L_{(i-1)j}$ on L_{ij}, $\mathbf{f}_{ij} = \left[f_{ijx}\ f_{ijy}\ f_{ijz}\right]^{\mathrm{T}}$
$\mathbf{f}_{(i+1)j}$	Force exerted by L_{ij} on $L_{(i+1)j}$, $\mathbf{f}_{(i+1)j} = \left[f_{(i+1)jx}\ f_{(i+1)jy}\ f_{(i+1)jz}\right]^{\mathrm{T}}$
$\boldsymbol{\tau}_{ij}$	Moment exerted by $L_{(i-1)j}$ on L_{ij} with respect to O_{ij}, $\boldsymbol{\tau}_{ij} = \tau_{ijx} \cdot \mathbf{X}_{ij} + \tau_{ijy} \cdot \mathbf{Y}_{ij}$
$\boldsymbol{\tau}_{(i+1)j}$	Moment exerted by L_{ij} on $L_{(i+1)j}$ with respect to $O_{(i+1)j}$, $\boldsymbol{\tau}_{(i+1)j} = \tau_{(i+1)jx} \cdot \mathbf{X}_{(i+1)j} + \tau_{(i+1)jy} \cdot \mathbf{Y}_{(i+1)j}$
$\mathbf{X}_{ij}$, $\mathbf{Y}_{ij}$, $\mathbf{Z}_{ij}$	The unit vectors directed along the x, y, z axis of $\mathcal{F}_{ij}$ represented in the frame $\mathcal{B}$
$\mathbf{r}_{(i,i+1)j}$	Vector from O_{ij} to $O_{(i+1)j}$
$\mathbf{r}_{(i,Ci)j}$	Vector from O_{ij} to center of mass C_{ij}
$\mathbf{r}_{B,ij}$	The vector from O_B to O_{ij}
$\mathbf{r}_{B,(i+1)j}$	The vector from O_B to $O_{(i+1)j}$
$\mathbf{r}_{B,Cij}$	The vector from O_B to the mass center C_{ij}

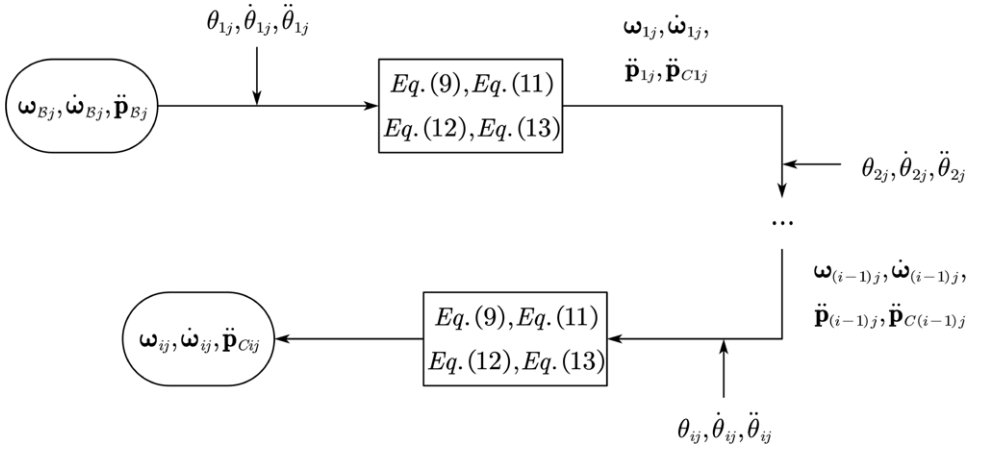

Figure 5. *Computational structure of the iterative algorithm.*

Before establishing the Newton–Euler equation for the jth leg, it is crucial to determine the forces and torques acting on this leg. These are shown in Fig. 6.

Fig. 6 shows that each link is subjected to two force vectors in unknown directions (each force vector can be decomposed into three unknown forces along the frame axes of the frame $\mathcal{B}$), And four torques, two under frame O_{ij} and others under frame $O_{(i+1)j}$ (in specific directions along their x and y axes). Links L_{2j} and L_{3j} are combined into a single link, which is defined as L_{sj}. Joints 1, 2, 5, and 6 are all R–joints. These R–joints have only one DOF, but five constraints. Hence, in the absence of consideration for reactive forces, an R-joint is subject to forces in three directions and torques in two directions. Joint 4 is an RP–joint, and its rotational and feed motions are coupled. The output torque of the motor can be converted from the supporting force in the direction of the feed. Thus, the supporting force in the direction of the feed f_{4jz} (along the z-axis of $\mathcal{F}_{4j}$) can be regarded as the actuated force. Therefore, joint 4 is subject to binding forces in two directions (x-axis and y-axis of $\mathcal{F}_{4j}$), the actuated force along the

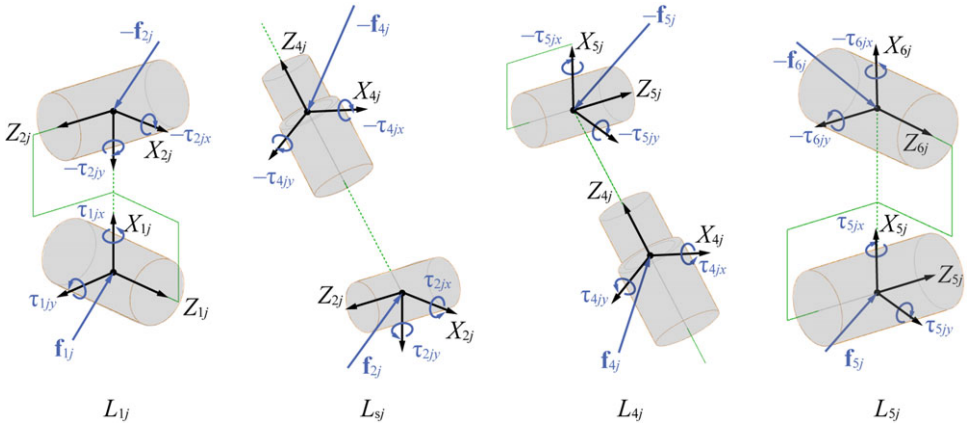

Figure 6. *Forces and torques on the links of the jth leg.*

feed direction, and constrained torques in two directions. In summary, each link is subjected to three unknown forces and two unknown torques, with a total of five unknown variables.

For each link, three Newton equations of constrained motion and three Euler equations of constrained rotation in space can be independently established, giving a total of six equations. Generally, each leg can be divided into four individual links, resulting in a total of 25 unknown variables related through 24 equivalent relationships.

Each leg has 25 unknown variables and 24 equations, giving 150 unknown variables and 144 equations for all six legs. For the MP, six expressions are obtained by the Newton–Euler equation. Therefore, we can establish a linear system with 150 equations for the whole PM.

4.1. Newton–Euler equations for a single leg

The jth leg ($j = 1 \sim 6$) can be divided into four links, denoted by L_{ij} ($i = 1, s, 4, 5$). The five joint origins are denoted by O_{ij} ($i = 1, 2, 4, 5, 6$). Each joint has five constraints, three unknown forces, and two unknown torques.

First, for link L_{1j}, the Newton–Euler equations are

$$\begin{cases} \mathbf{f}_{1j} - \mathbf{f}_{2j} + m_{1j}\mathbf{g} = m_{1j}\ddot{\mathbf{p}}_{C1j} \\ \boldsymbol{\tau}_{\mathbf{1j}} - \boldsymbol{\tau}_{\mathbf{2j}} + \tilde{\mathbf{r}}_{B,1j} \cdot \mathbf{f}_{1j} - \tilde{\mathbf{r}}_{B,2j} \cdot \mathbf{f}_{2j} + m_{1j}\tilde{\mathbf{r}}_{B,C1j}\mathbf{g} - m_{1j}\tilde{\mathbf{r}}_{B,C1j}\ddot{\mathbf{p}}_{C1j} = \dfrac{d}{dt}\left(\mathbf{I}_{1j}\boldsymbol{\omega}_{1j}\right) \end{cases} \tag{14}$$

$\tilde{\mathbf{r}}_{B,1j}$ is the skew-symmetric matrix of $\mathbf{r}_{B,1j}$:

$$\mathbf{r}_{B,1j} = \begin{bmatrix} r_{1jx} & r_{1jy} & r_{1jz} \end{bmatrix},$$

and

$$\tilde{\mathbf{r}}_{B,1j} = \begin{bmatrix} 0 & -r_{1jz} & r_{1jy} \\ r_{1jz} & 0 & -r_{1jx} \\ -r_{1jy} & r_{1jx} & 0 \end{bmatrix}.$$

All vector expressions with a tilde in the following text are similar.

$\mathbf{I}_{1j}$ is the inertia tensor of L_{1j} under the frame $\mathcal{B}$. According to the coordinate transformation rules for the inertia tensor,

$$\mathbf{I}_{1j} = \mathbf{R}_{O_{C1j}} \cdot^{O_{C1j}} \mathbf{I}_{1j} \cdot \mathbf{R}_{O_{C1j}}^{\mathrm{T}}$$

where ${}^{O_{1j}}\mathbf{I}_{1j}$ is the inertia tensor of L_{1j} concerning the reference frame of the center of mass of link $1j$, which is a constant matrix. $\mathbf{R}_{O_{C1j}}$ is the transformation matrix from the mass center reference frame to the frame $\mathcal{B}$.

Similarly, the Newton–Euler equations of L_{4j} and L_{5j} are

$$\begin{cases} \mathbf{f}_{4j} - \mathbf{f}_{5j} + m_{4j}\mathbf{g} = m_{4j}\ddot{\mathbf{p}}_{C4j} \\ \boldsymbol{\tau}_{4j} - \boldsymbol{\tau}_{5j} + \tilde{\mathbf{r}}_{B,4j} \cdot \mathbf{f}_{4j} - \tilde{\mathbf{r}}_{B,5j} \cdot \mathbf{f}_{5j} + m_{4j}\tilde{\mathbf{r}}_{B,C4j}\mathbf{g} - m_{4j}\tilde{\mathbf{r}}_{B,C4j}\ddot{\mathbf{p}}_{C4j} = \dfrac{d}{dt}\left(\mathbf{I}_{4j}\boldsymbol{\omega}_{4j}\right) \end{cases} \tag{15}$$

and

$$\begin{cases} \mathbf{f}_{5j} - \mathbf{f}_{6j} + m_{5j}\mathbf{g} = m_{5j}\ddot{\mathbf{p}}_{C5j} \\ \boldsymbol{\tau}_{5j} - \boldsymbol{\tau}_{6j} + \tilde{\mathbf{r}}_{B,5j} \cdot \mathbf{f}_{5j} - \tilde{\mathbf{r}}_{B,6j} \cdot \mathbf{f}_{6j} + m_{5j}\tilde{\mathbf{r}}_{B,C5j}\mathbf{g} - m_{5j}\tilde{\mathbf{r}}_{B,C5j}\ddot{\mathbf{p}}_{C5j} = \dfrac{d}{dt}\left(\mathbf{I}_{5j}\boldsymbol{\omega}_{5j}\right) \end{cases} \tag{16}$$

For L_{sj}, we have

$$\begin{cases} \mathbf{f}_{2j} - \mathbf{f}_{4j} + \sum_{i=2}^{3} m_{ij}\mathbf{g} = \sum_{i=2}^{3} m_{ij}\ddot{\mathbf{p}}_{Cij} \\ \boldsymbol{\tau}_{2j} - \boldsymbol{\tau}_{4j} + \tilde{\mathbf{r}}_{B,2j} \cdot \mathbf{f}_{2j} - \tilde{\mathbf{r}}_{B,4j} \cdot \mathbf{f}_{4j} \\ \qquad\qquad + \sum_{i=2}^{3} \left(m_{ij}\tilde{\mathbf{r}}_{B,Cij}\mathbf{g} - m_{ij}\tilde{\mathbf{r}}_{B,Cij}\ddot{\mathbf{p}}_{Cij}\right) = \sum_{i=2}^{3} \frac{d}{dt}\left(\mathbf{I}_{ij}\boldsymbol{\omega}_{ij}\right) \end{cases} \tag{17}$$

Rearranging Eqs. (14), (15), (16), and (17) gives

$$\begin{cases} \mathbf{f}_{1j} - \mathbf{f}_{2j} = m_{1j}\left(\ddot{\mathbf{p}}_{C1j} - \mathbf{g}\right) \\ \mathbf{f}_{2j} - \mathbf{f}_{4j} = \sum_{i=2}^{3} m_{ij}\left(\ddot{\mathbf{p}}_{Cij} - \mathbf{g}\right) \\ \mathbf{f}_{4j} - \mathbf{f}_{5j} = m_{4j}\left(\ddot{\mathbf{p}}_{C4j} - \mathbf{g}\right) \\ \mathbf{f}_{5j} - \mathbf{f}_{6j} = m_{5j}\left(\ddot{\mathbf{p}}_{C5j} - \mathbf{g}\right) \\ \tilde{\mathbf{r}}_{B,1j} \cdot \mathbf{f}_{1j} - \tilde{\mathbf{r}}_{B,2j} \cdot \mathbf{f}_{2j} + \boldsymbol{\tau}_{1j} - \boldsymbol{\tau}_{2j} = \frac{d}{dt}\left(\mathbf{I}_{1j}\boldsymbol{\omega}_{1j}\right) + m_{1j}\tilde{\mathbf{r}}_{B,C1j}\left(\ddot{\mathbf{p}}_{C1j} - \mathbf{g}\right) \\ \tilde{\mathbf{r}}_{B,2j} \cdot \mathbf{f}_{2j} - \tilde{\mathbf{r}}_{B,4j} \cdot \mathbf{f}_{4j} + \boldsymbol{\tau}_{2j} - \boldsymbol{\tau}_{4j} = \sum_{i=2}^{3}\left[\frac{d}{dt}\left(\mathbf{I}_{ij}\boldsymbol{\omega}_{ij}\right) + m_{ij}\tilde{\mathbf{r}}_{B,Cij}\left(\ddot{\mathbf{p}}_{Cij} - \mathbf{g}\right)\right] \\ \tilde{\mathbf{r}}_{B,4j} \cdot \mathbf{f}_{4j} - \tilde{\mathbf{r}}_{B,5j} \cdot \mathbf{f}_{5j} + \boldsymbol{\tau}_{4j} - \boldsymbol{\tau}_{5j} = \frac{d}{dt}\left(\mathbf{I}_{4j}\boldsymbol{\omega}_{4j}\right) + m_{4j}\tilde{\mathbf{r}}_{B,C4j}\left(\ddot{\mathbf{p}}_{C4j} - \mathbf{g}\right) \\ \tilde{\mathbf{r}}_{B,5j} \cdot \mathbf{f}_{5j} - \tilde{\mathbf{r}}_{B,6j} \cdot \mathbf{f}_{6j} + \boldsymbol{\tau}_{5j} - \boldsymbol{\tau}_{6j} = \frac{d}{dt}\left(\mathbf{I}_{5j}\boldsymbol{\omega}_{5j}\right) + m_{5j}\tilde{\mathbf{r}}_{B,C5j}\left(\ddot{\mathbf{p}}_{C5j} - \mathbf{g}\right) \end{cases} \tag{18}$$

In Eq. (18), we arrange all unknown variables on the left and all known parts on the right.

4.2. Newton–Euler equations for the MP

The MP is a link connecting the ends of the six legs. Any external loads acting on the MP are simplified as a force $\mathbf{F}_e$ and a torque $\mathbf{M}_e$ under the frame $\mathcal{B}$. Moreover, the MP is constrained by six R–joints at the leg–MP connections O_{Pj}, each containing three forces and two torques. Thus, the dynamic equations are written as:

$$\begin{cases} \sum_{j=1}^{6} \mathbf{f}_{6j} - \mathbf{F}_e + m_{MP}\mathbf{g} = m_{MP}\ddot{\mathbf{p}}_{CMP} \\ \sum_{j=1}^{6}\left(\tilde{\mathbf{r}}_{B,6j} \cdot \mathbf{f}_{6j} + \boldsymbol{\tau}_{6j}\right) - \tilde{\mathbf{r}}_{B,P} \cdot \mathbf{F}_e - \mathbf{M}_e \\ \qquad\qquad + m_{MP}\tilde{\mathbf{r}}_{B,CMP}\mathbf{g} - m_{MP}\tilde{\mathbf{r}}_{B,CMP}\ddot{\mathbf{p}}_{CMP} = \frac{d}{dt}\left(\mathbf{I}_{MP}\boldsymbol{\omega}_{MP}\right) \end{cases} \tag{19}$$

where

$$\mathbf{I}_{MP} = \mathbf{R}_{COP} \cdot {}^{COP}\mathbf{I}_{MP} \cdot \mathbf{R}_{COP}^{\mathrm{T}}$$

is the inertia tensor of the MP under the frame $\mathcal{B}$; the terms $\mathbf{R}_{COP}$ and ${}^{COP}\mathbf{I}_{MP}$ are similar to those in previous equations.

Rearranging Eq. (19), we obtain the following:

$$\begin{cases} \sum_{j=1}^{6} \mathbf{f}_{6j} = m_{MP}\left(\ddot{\mathbf{p}}_{CMP} - \mathbf{g}\right) + \mathbf{F}_e \\ \sum_{j=1}^{6} \left(\tilde{\mathbf{r}}_{B,6j} \cdot \mathbf{f}_{6j} + \boldsymbol{\tau}_{6j}\right) = \frac{d}{dt}\left(\mathbf{I}_{MP}\boldsymbol{\omega}_{MP}\right) + \tilde{\mathbf{r}}_{B,P} \cdot \mathbf{F}_e + \mathbf{M}_e + m_{MP}\tilde{\mathbf{r}}_{B,CMP}\left(\ddot{\mathbf{p}}_{CMP} - \mathbf{g}\right) \end{cases} \tag{20}$$

4.3. Solution for the actuated force

Combining Eqs. (18) and (20) yields the Newton–Euler equations of the whole PM:

$$\begin{bmatrix} \mathbf{F}_1 - \mathbf{F}_2 \\ \mathbf{F}_2 - \mathbf{F}_4 \\ \mathbf{F}_4 - \mathbf{F}_5 \\ \mathbf{F}_5 - \mathbf{F}_6 \\ \sum_{j=1}^{6} \mathbf{f}_{6j} \\ \tilde{\mathbf{r}}_{B,1} \cdot \mathbf{F}_1 - \tilde{\mathbf{r}}_{B,2} \cdot \mathbf{F}_2 + \boldsymbol{\mu}_1 - \boldsymbol{\mu}_2 \\ \tilde{\mathbf{r}}_{B,2} \cdot \mathbf{F}_2 - \tilde{\mathbf{r}}_{B,4} \cdot \mathbf{F}_4 + \boldsymbol{\mu}_2 - \boldsymbol{\mu}_4 \\ \tilde{\mathbf{r}}_{B,4} \cdot \mathbf{F}_4 - \tilde{\mathbf{r}}_{B,5} \cdot \mathbf{F}_5 + \boldsymbol{\mu}_4 - \boldsymbol{\mu}_5 \\ \tilde{\mathbf{r}}_{B,5} \cdot \mathbf{F}_5 - \tilde{\mathbf{r}}_{B,6} \cdot \mathbf{F}_6 + \boldsymbol{\mu}_5 - \boldsymbol{\mu}_6 \\ \sum_{j=1}^{6} \left(\tilde{\mathbf{r}}_{B,6j} \cdot \mathbf{f}_{6j} + \boldsymbol{\tau}_{6j}\right) \end{bmatrix} = \begin{bmatrix} \mathbf{G}_1 \\ \mathbf{G}_2 + \mathbf{G}_3 \\ \mathbf{G}_4 \\ \mathbf{G}_5 \\ \mathbf{G}_{MP} + \mathbf{F}_e \\ \mathbf{N}_1 + \boldsymbol{\mu}_{C1} \\ \mathbf{N}_2 + \mathbf{N}_3 + \boldsymbol{\mu}_{C2} + \boldsymbol{\mu}_{C3} \\ \mathbf{N}_4 + \boldsymbol{\mu}_{C4} \\ \mathbf{N}_5 + \boldsymbol{\mu}_{C5} \\ \mathbf{N}_{MP} + \boldsymbol{\mu}_{CMP} + \tilde{\mathbf{r}}_{B,P} \cdot \mathbf{F}_e + \mathbf{M}_e \end{bmatrix} \tag{21}$$

The elements of Eq. (21) are as follows:

On the left-hand side:

$$\mathbf{F}_i = \left[\mathbf{f}_{i1}^{\mathrm{T}}\ \mathbf{f}_{i2}^{\mathrm{T}}\ \mathbf{f}_{i3}^{\mathrm{T}}\ \mathbf{f}_{i4}^{\mathrm{T}}\ \mathbf{f}_{i5}^{\mathrm{T}}\ \mathbf{f}_{i6}^{\mathrm{T}}\right]_{18\times 1}^{\mathrm{T}}$$

$$\boldsymbol{\mu}_i = \left[\boldsymbol{\tau}_{i1}^{\mathrm{T}}\ \boldsymbol{\tau}_{i2}^{\mathrm{T}}\ \boldsymbol{\tau}_{i3}^{\mathrm{T}}\ \boldsymbol{\tau}_{i4}^{\mathrm{T}}\ \boldsymbol{\tau}_{i5}^{\mathrm{T}}\ \boldsymbol{\tau}_{i6}^{\mathrm{T}}\right]_{18\times 1}^{\mathrm{T}}$$

$$\tilde{\mathbf{r}}_{B,i} = \left[\tilde{\mathbf{r}}_{B,i1}^{\mathrm{T}}\ \tilde{\mathbf{r}}_{B,i2}^{\mathrm{T}}\ \tilde{\mathbf{r}}_{B,i3}^{\mathrm{T}}\ \tilde{\mathbf{r}}_{B,i4}^{\mathrm{T}}\ \tilde{\mathbf{r}}_{B,i5}^{\mathrm{T}}\ \tilde{\mathbf{r}}_{B,i6}^{\mathrm{T}}\right]_{18\times 3}^{\mathrm{T}}$$

On the right-hand side, $\mathbf{G}_i$ is the inertia forces vector composed of the inertia forces of links L_{ij} ($j = 1 \sim 6$) and $\mathbf{G}_{MP}$ is the inertia force of the MP:

$$\mathbf{G}_i = \begin{bmatrix} m_{i1}\left(\ddot{\mathbf{p}}_{Ci1} - \mathbf{g}\right) \\ m_{i2}\left(\ddot{\mathbf{p}}_{Ci2} - \mathbf{g}\right) \\ \vdots \\ m_{i6}\left(\ddot{\mathbf{p}}_{Ci6} - \mathbf{g}\right) \end{bmatrix}_{18\times 1}$$

$$\mathbf{G}_{MP} = \left[m_{MP}\left(\ddot{\mathbf{p}}_{CMP} - \mathbf{g}\right)\right]_{3\times 1}$$

Then, $\boldsymbol{\mu}_{Ci}$ represents the moment vector due to gravity of links L_{ij} ($j = 1 \sim 6$). $\boldsymbol{\mu}_{\mathrm{CMP}}$ is similar.

$$\boldsymbol{\mu}_{Ci} = \begin{bmatrix} m_{i1}\tilde{\mathbf{r}}_{B,Ci1}\,(\ddot{\mathbf{p}}_{Ci1} - \mathbf{g}) \\ m_{i2}\tilde{\mathbf{r}}_{B,Ci2}\,(\ddot{\mathbf{p}}_{Ci2} - \mathbf{g}) \\ \vdots \\ m_{i6}\tilde{\mathbf{r}}_{B,Ci6}\,(\ddot{\mathbf{p}}_{Ci6} - \mathbf{g}) \end{bmatrix}_{18\times 1}$$

$$\boldsymbol{\mu}_{CMP} = [m_{MP}\tilde{\mathbf{r}}_{B,CMP}\,(\ddot{\mathbf{p}}_{CMP} - \mathbf{g})\,]_{3\times 1}$$

Under the theorem of the moment of momentum, $\mathbf{N}_i$ represents the differential angular momentum vector of links L_{ij} ($j = 1 \sim 6$) and $\mathbf{N}_{MP}$ is the differential angular momentum of the MP:

$$\mathbf{N}_i = \begin{bmatrix} \dfrac{d}{dt}(\mathbf{I}_{i1}\boldsymbol{\omega}_{i1}) \\ \dfrac{d}{dt}(\mathbf{I}_{i2}\boldsymbol{\omega}_{i2}) \\ \vdots \\ \dfrac{d}{dt}(\mathbf{I}_{i6}\boldsymbol{\omega}_{i6}) \end{bmatrix}_{18\times 1}$$

$$\mathbf{N}_{MP} = \left[\frac{d}{dt}(\mathbf{I}_{MP}\boldsymbol{\omega}_{MP})\right]_{3\times 1}$$

Rearranging Eq. (21) and rewriting it in matrix form, we obtain the following:

$$\mathbf{A} = \begin{bmatrix} \mathbf{I}_{18} & -\mathbf{I}_{18} & & & & & & & & & \\ & \mathbf{I}_{18} & -\mathbf{I}_{18} & & & & & & & & \\ & & \mathbf{I}_{18} & -\mathbf{I}_{18} & & & & & & & \\ & & & \mathbf{I}_{18} & -\mathbf{I}_{18} & & & & & & \\ & & & & \mathbf{I}_{3,18} & & & & & & \\ \tilde{\mathbf{r}}_{\mathrm{B},1} & -\tilde{\mathbf{r}}_{\mathrm{B},2} & & & & \mathbf{e}_1 & -\mathbf{e}_2 & & & & \\ & \tilde{\mathbf{r}}_{\mathrm{B},2} & -\tilde{\mathbf{r}}_{\mathrm{B},4} & & & & \mathbf{e}_2 & -\mathbf{e}_4 & & & \\ & & \tilde{\mathbf{r}}_{\mathrm{B},4} & -\tilde{\mathbf{r}}_{\mathrm{B},5} & & & & \mathbf{e}_4 & -\mathbf{e}_5 & & \\ & & & \tilde{\mathbf{r}}_{\mathrm{B},5} & -\tilde{\mathbf{r}}_{\mathrm{B},6} & & & & \mathbf{e}_5 & -\mathbf{e}_6 \\ & & & & \mathbf{S}\mathbf{r}_{\mathrm{B},6} & & & & & \mathbf{S}\mathbf{e}_6 \end{bmatrix}_{150\times 150} \tag{22}$$

where $\mathbf{I}_{18}$ denotes the identity matrix of order 18 and

$$\mathbf{I}_{3,18} = \begin{bmatrix} \mathbf{I}_3 & \cdots & \mathbf{I}_3 \end{bmatrix}_{3\times 18}$$

The orientations of the torques on the links are

$$\mathbf{e}_i = \begin{bmatrix} \mathbf{X}_{i1} & \mathbf{Y}_{i1} & & & & & \\ & & \mathbf{X}_{i2} & \mathbf{Y}_{i2} & & & \\ & & & & \ddots & \ddots & \\ & & & & & \mathbf{X}_{i6} & \mathbf{Y}_{i6} \end{bmatrix}_{18\times 12}$$

and

$$\mathbf{Sr}_{\mathrm{B},6} = \left[\tilde{\mathbf{r}}_{\mathrm{B},61}\ \tilde{\mathbf{r}}_{\mathrm{B},62}\ \cdots\ \tilde{\mathbf{r}}_{\mathrm{B},65}\ \tilde{\mathbf{r}}_{\mathrm{B},66}\right]_{3\times 18}$$

$$\mathbf{Se}_6 = \left[\mathbf{X}_{61}\ \mathbf{Y}_{61}\ \cdots\ \mathbf{X}_{66}\ \mathbf{Y}_{66}\right]_{3\times 12}$$

Here,

$$\mathbf{x} = \left[\mathbf{F}_1^{\mathrm{T}}\ \mathbf{F}_2^{\mathrm{T}}\ \mathbf{F}_4^{\mathrm{T}}\ \mathbf{F}_5^{\mathrm{T}}\ \mathbf{F}_6^{\mathrm{T}}\ \boldsymbol{\tau}_1^{\mathrm{T}}\ \boldsymbol{\tau}_2^{\mathrm{T}}\ \boldsymbol{\tau}_4^{\mathrm{T}}\ \boldsymbol{\tau}_5^{\mathrm{T}}\ \boldsymbol{\tau}_6^{\mathrm{T}}\right]^{\mathrm{T}}_{150\times 1} \tag{23}$$

where $\boldsymbol{\tau}_i = \left[\tau_{i1x}\ \tau_{i1y}\ \tau_{i2x}\ \tau_{i2y}\ \cdots\ \tau_{i6x}\ \tau_{i6y}\right]^{\mathrm{T}}_{12\times 1}$. The vector $\mathbf{x}$ contains 150 elements, where elements 37–54 contain the required actuated forces.

All terms of $\mathbf{b}$ are known values on the right side of Eq. (21). Therefore, Eq. (21) can be rewritten as:

$$\mathbf{A}\cdot\mathbf{x} = \mathbf{b} \tag{24}$$

As long as the PM is not in a singular configuration or has actuated redundancy, matrix A is a full-rank matrix, $|\mathbf{A}| \neq 0$, and the system of equations has a unique solution. Furthermore, approximately 95.68% of the elements in the matrix are zeros, indicating that it is a sparse matrix. To improve solving speed, it can be converted into a sparse matrix during computations, and the GMRES [36] can be used.

Thus, we choose $\mathbf{x}_0 \in \mathbb{R}^{150\times 1}$ as an initial vector and set

$$\mathbf{r}_0 = \mathbf{b} - \mathbf{A}\mathbf{x}_0, \quad \mathbf{v}_1 = \frac{\mathbf{r}_0}{\|\mathbf{r}_0\|}, \quad \beta = ||\mathbf{r}_0||$$

And then, use the Arnoldi process, for $n = 1, 2, \cdots, k, \cdots$, we do

$$h_{m,n} = (\mathbf{A}\mathbf{v}_n)^{\mathrm{T}}\mathbf{v}_m, \quad m = 1, 2, \cdots, n$$

$$\hat{\mathbf{v}}_{n+1} = \mathbf{A}\mathbf{v}_n - \sum_{m=1}^{n} h_{m,n}\mathbf{v}_m$$

$$h_{n+1,n} = ||\hat{\mathbf{v}}_{n+1}||$$

$$\mathbf{v}_{n+1} = \hat{\mathbf{v}}_{n+1}/h_{n+1,n}$$

until $h_{n+1,n} < \epsilon$. ϵ is the upper limit of the error based on the specific situation.

And we can get the orthonormal basis $\mathbf{V}_k = [\mathbf{v_1}, \ldots, \mathbf{v}_k]_{150\times k}$ and the matrix elements $h_{m,n}$ form the matrix $\mathbf{H}_k \in \mathbb{R}^{(k+1)\times k}$.

Solve the linear least squares as:

$$\min||\beta\mathbf{e} - \mathbf{H}_k\mathbf{y}_k||\,, \tag{25}$$

and $\mathbf{e} = [1, 0, \cdots, 0]_{(k+1)\times 1}$. Note the result as $\mathbf{y}_k$.

Finally, the numerical solution

$$\mathbf{x} = \mathbf{x}_0 + \mathbf{V}_k\mathbf{y}_k\,. \tag{26}$$

The set of actuated forces is denoted as $\mathbf{F}_{4jz}$:

$$\mathbf{F}_{4jz} = \left[f_{41z}\ \ldots\ f_{46z}\right]^{\mathrm{T}}, \tag{27}$$

where

$$f_{4jz} = \left[\mathbf{x}\,(34+3j)\ \ \mathbf{x}\,(35+3j)\ \ \mathbf{x}\,(36+3j)\right]\cdot\mathbf{Z}_{4j}$$

Table II. *Structure parameters of PM for numerical simulations.*

Variable	H_p	H	H_b	r_p	r_b	U_p	U_b
(m)	0.026	0.295	0.027	0.125	0.160	0.010	0.010
	θ_p	θ_b					
(deg)	24	96					

Table III. *Dynamic parameters of PM for numerical simulations.*

		L_{1j}	L_{2j}	L_{3j}
Mass (kg)		0.155	2	0.43
Center of mass (m)		$\begin{bmatrix} 0.005 \\ 0 \\ 0 \end{bmatrix}$	$\begin{bmatrix} 0 \\ -0.067 \\ 0 \end{bmatrix}$	$\begin{bmatrix} 0 \\ 0 \\ 0.133 \end{bmatrix}$
Inertia tensor (kg · m^2,	$\begin{bmatrix} I_{xx} \\ I_{yy} \\ I_{zz} \end{bmatrix}$	$\begin{bmatrix} 2.5 \times 10^{-5} \\ 2.6 \times 10^{-5} \\ 2.6 \times 10^{-5} \end{bmatrix}$	$\begin{bmatrix} 3.2 \times 10^{-3} \\ 2.1 \times 10^{-3} \\ 3.2 \times 10^{-3} \end{bmatrix}$	$\begin{bmatrix} 8.8 \times 10^{-4} \\ 8.8 \times 10^{-4} \\ 3 \times 10^{-5} \end{bmatrix}$
		L_{4j}	L_{5j}	MP
		0.8	0.155	3.5
		$\begin{bmatrix} 0 \\ 0 \\ -0.066 \end{bmatrix}$	$\begin{bmatrix} 0.005 \\ 0 \\ 0 \end{bmatrix}$	$\begin{bmatrix} 0 \\ 0 \\ -0.011 \end{bmatrix}$
		$\begin{bmatrix} 1.4 \times 10^{-3} \\ 1.4 \times 10^{-3} \\ 3.2 \times 10^{-3} \end{bmatrix}$	$\begin{bmatrix} 2.5 \times 10^{-5} \\ 2.6 \times 10^{-5} \\ 2.6 \times 10^{-5} \end{bmatrix}$	$\begin{bmatrix} 2.5 \times 10^{-2} \\ 2.5 \times 10^{-2} \\ 4.8 \times 10^{-2} \end{bmatrix}$

5. Simulations

To validate the correctness of the dynamics of the 6-RR-RP-RR PM, we compare the results of the mathematical dynamic model with those of a simulation model. The model described in this paper consists of both inverse kinematics and inverse dynamics. The simulation model, which is established using the automatic dynamic analysis of multibody systems software, provides both kinematic and dynamic solutions through various probes.

First, the structure parameters of the PM must be defined. From Fig. 2, these parameters are as listed in Table II. And their dynamic parameters are as listed in Table III.

To verify the accuracy of the algorithm and facilitate computation, the specific parameters of the actual PM are simplified to ideal parameters in the simulation. $\left[I_{xy}, I_{xz}, I_{yz}\right]^{\mathrm{T}} = [0, 0, 0]^{\mathrm{T}}$

The MP has 6-DOFs in space and consists of translation and rotation motions along the three directions of the frame $\mathcal{B}$. Let the MP move along the spiral line, with arbitrary angle changes in the motion process. The parametric equations of the trajectory under the frame $\mathcal{B}$ are

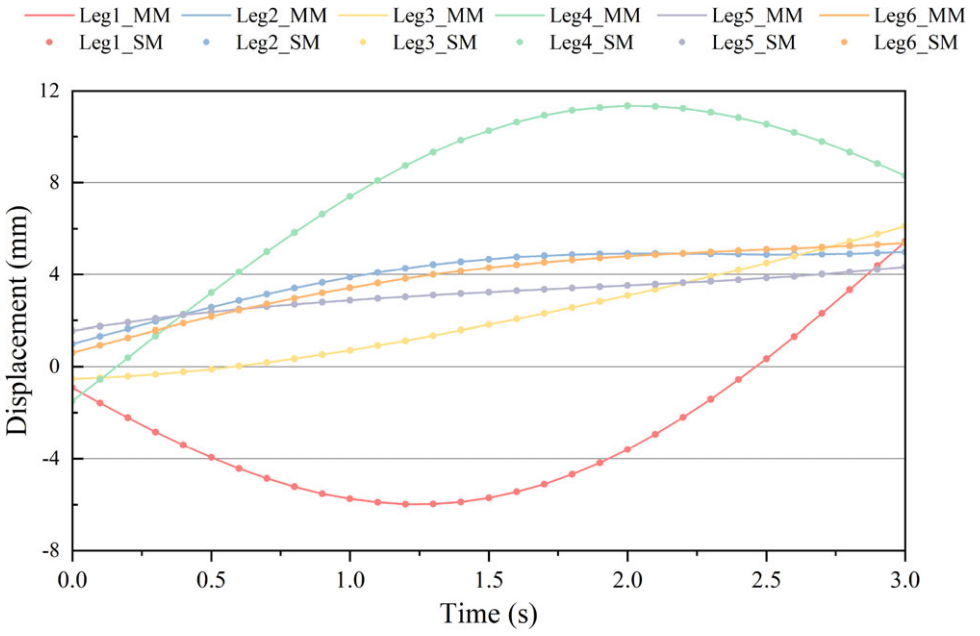

Figure 7. *Kinematic comparison (MM – mathematical model, SM – simulation model).*

$$\begin{cases} p_x = 0.005\sin(t) & (m) \\ p_y = 0.005\cos(t) & (m) \\ p_z = 0.002\,t & (m) \\ \varphi = \frac{\pi}{180}\sin(t) & (rad) \\ \theta = \frac{2\pi}{180}\sin(t) & (rad) \\ \psi = \frac{5\pi}{180}\sin(t) & (rad) \end{cases} \tag{28}$$

The displacement trajectory comparison is illustrated in Fig. 7. From the figure, it is evident that the mathematical results closely align with the simulations.

From such a complex trajectory, we can learn how the algorithm performs in a real-world condition rather than in a well-designed environment. Furthermore, we conducted simulations under three different operating conditions to validate the correctness of the algorithm, and these conditions are presented in Table IV.

The spiral trajectory equation has illustrated as Eq. (28), and the acceleration of gravity is as follows:

$$\mathbf{g} = [0, 0, -9.8]^{\mathrm{T}}\ (m/s^2).$$

And the external action contains a force vector $\mathbf{F}_e^{\mathcal{P}}$ and a torque vector $\mathbf{M}_e^{\mathcal{P}}$, which executed on the frame $\mathcal{P}$, as:

$$\mathbf{F}_e^{\mathcal{P}} = [10\sin(t), 10\cos(t), -10\sin(t)]^{\mathrm{T}}\ (N), \quad \mathbf{M}_e^{\mathcal{P}} = [\sin(t), 2\cos(t), 3\sin(t)]^{\mathrm{T}}\ (N \cdot m),$$

$$\mathbf{F}_e = \mathbf{T}_{\mathcal{P}} \cdot \mathbf{F}_e^{\mathcal{P}}, \qquad \mathbf{M}_e = \mathbf{T}_{\mathcal{P}} \cdot \mathbf{M}_e^{\mathcal{P}}.$$

In Condition 1, we consider the influence of inertia forces resulting from motion on the actuated force, while disregarding gravity and external actions. As shown in Fig. 8, the graph simultaneously

Table IV. *Three different operating conditions.*

	Condition 1	Condition 2	Condition 3
Total time (s)		$t = 3$	
Step length (s)		$\Delta t = 0.1$	
Spiral trajectory	√	√	√
Gravity	×	√	√
External action	×	×	√

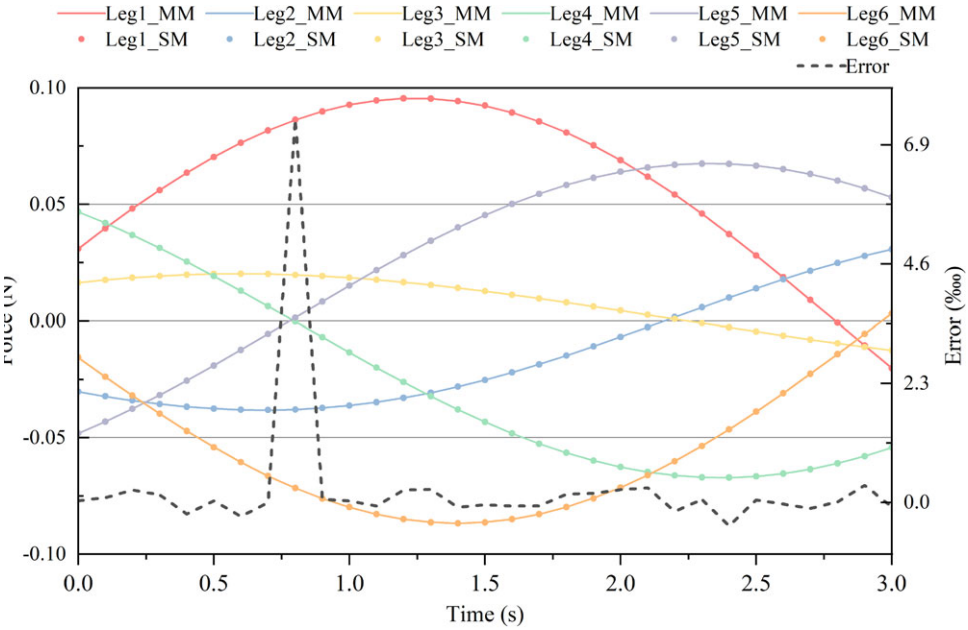

Figure 8. *Condition 1, a comparison of the models considering only inertia forces.*

includes the actuated force curves of both the mathematical model (MM) and the simulation model (SM). The right-hand coordinate system in the graph represents the average relative error between the two models. This means obtaining the relative error between the two models for each individual leg and then averaging these relative errors across the six legs. The error exhibits a random zigzag pattern, unrelated to inertia forces and motion conditions, with magnitudes at the order of 10^{-4}. The spike observed at $0.8s$ is considered arising as the actuated force approaches zero. Therefore, the algorithm remains reliable when considering only inertia forces.

In Condition 2, both inertia forces and gravity are considered simultaneously. As shown in Fig. 9, the actuated forces noticeably increase. And since gravity acceleration is a constant value unaffected by simulation software computation errors, the error between the simulation results and the mathematical model significantly decreases. Furthermore, both models remain consistent, indicating that the algorithm remains reliable.

Finally, in Condition 3, as shown in Fig. 10, inertia forces, gravity, and external actions are taken into account. As a result, actuated forces increase further, but the magnitude of the error has not changed significantly. Hence, the primary factor contributing to the error is presumably the acceleration error of the simulation.

In summary, we can conclude that the algorithm can be considered reliable, and the error is unrelated to motion.

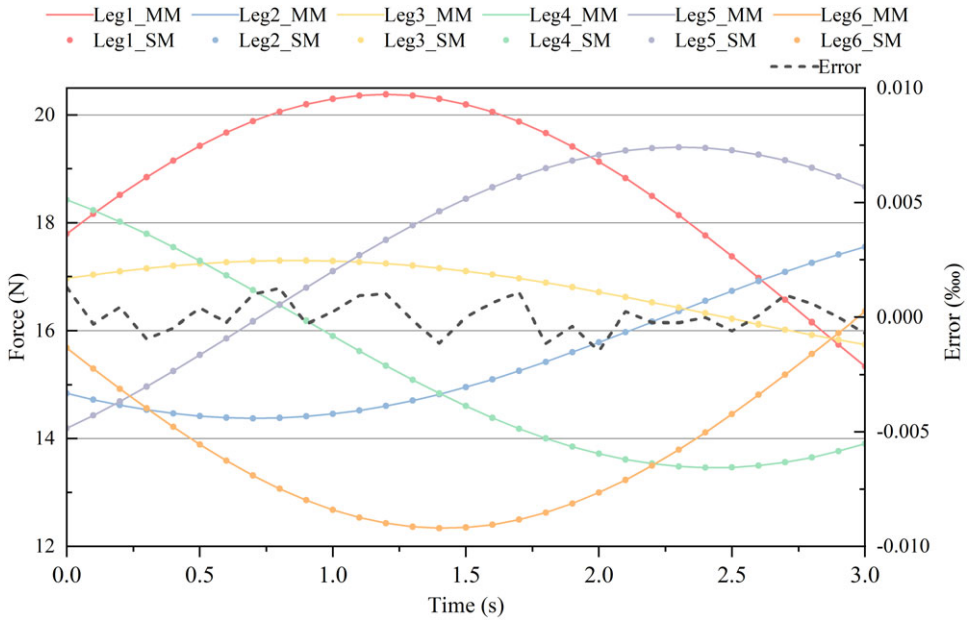

Figure 9. *Condition 2, a comparison of the models considering both inertia forces and gravity.*

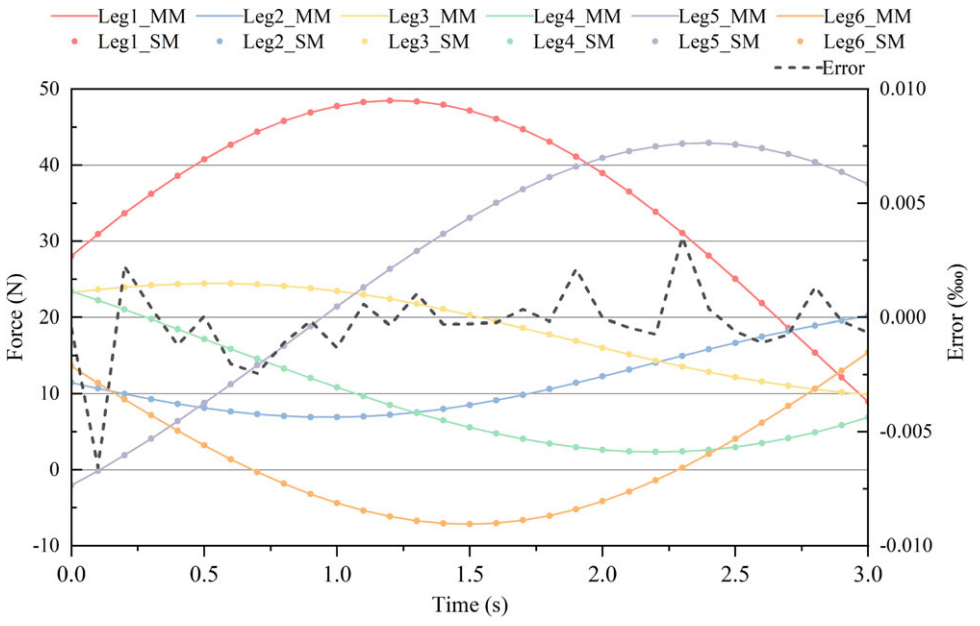

Figure 10. *Condition 3, a comparison of the models considering inertia forces, gravity, and external actions.*

6. Conclusion

This paper has described the inverse dynamic analysis of a 6-RR-RP-RR PM with offset universal joints. The introduction of RR–joints means that the dynamic model must be represented as an implicit system of equations. Based on the existing inverse kinematic model, this study established an iterative algorithm using rigid body velocity transformations, resulting in the velocity and acceleration input parameters of

all links in the base frame. The Newton–Euler method was then used to analyze the inverse dynamics of the PM, and dynamic equations for all links were established in the form of a equation system containing 150 unknowns and 150 equations. By solving the equation system, a vector **X** containing all joint forces and torques, including the desired actuated force $\mathbf{F}_{4jz}$, was obtained. The correctness of the mathematical model was verified through numerical simulations using the automatic dynamic analysis of multibody systems software. The algorithm closely aligns with the simulation and is deemed reliable. The derived equations can be used to determine the forces acting on all joints of the PM. They are not only useful for calculating the actuated force and force control, but also for structural optimization of PMs. In future research, the effect of friction will be studied by introducing dissipative forces into each Euler dynamic equation, and the PM will be validated through experiments.

Author contributions. Hasiaoqier Han concevied the study. Qingwen Wu and Huze Huang designed the study. Dawei Li and Huze Huang performed simulation analyses. Hasiaoqier Han and Zhenbang Xu derived the part of kinematics, and Huze Huang derived the part of dynamics. Huze Huang wrote the article.

Financial support. This work was supported by the National Natural Science Foundation of China [Grant Nos. 52005478, 62235018] and the Youth Innovation Promotion Association, Chinese Academy of Sciences [Grant No. 2022215].

Competing interests. All authors disclosed no relevant relationships.

Ethical approval. None.

References

[1] V. E. Gough, "Universal Tyre Test Machine," **In:** *Proceedings of the FISITA 9th International Technical Congress*, London (1962) 117–137.
[2] D. Stewart, "A platform with six degrees of freedom," *Proceed Inst Mech Eng* **180**(1), 371–386 (1965).
[3] R. Gloess and B. Lula, Challenges of extreme load hexapod design and modularization for large ground-based telescopes, San Diego, California, USA, (2010) 77391U.
[4] K. Großmann and B. Kauschinger, "Eccentric universal joints for parallel kinematic machine tools: Variants and kinematic transformations," *Prod Engineer* **6**(4-5), 521–529 (2012).
[5] B. Hu and Y. Lu, "Analyses of kinematics, statics, and workspace of a 3-RRPRR parallel manipulator and its three isomeric mechanisms," *Proceed Inst Mech Eng, Part C: J Mech Eng Sci* **222**(9), 1829–1837 (2008).
[6] M. M. Dalvand and B. Shirinzadeh, "Kinematics analysis of 6-DOF parallel micro-manipulators with offset U-joints: A case study," *Inter J Intell Mechatro Robot* **2**(1), 28–40 (2012).
[7] M. M. Dalvand, B. Shirinzadeh and S. Nahavandi, "Inverse Kinematics Analysis of 6-RRCRR Parallel Manipulators," **In:** *2013 IEEE/ASME International Conference on Advanced Intelligent Mechatronics*, Wollongong, NSW (IEEE, 2013) pp. 644–648.
[8] H.-S.-A.-Q.-E. Han, C.-Y. Han, Z.-B. Xu, M.-C. Zhu, Y. Yu and Q.-W. Wu, "Kinematics analysis and testing of novel 6- P -RR-R-RR parallel platform with offset RR-joints," *Proceed Inst Mech Eng, Part C: J Mech Eng Sci* **233**(10), 3512–3530 (2019).
[9] H. Han, Y. Zhang, H. Zhang, C. Han, A. Li and Z. Xu, "Kinematic analysis and performance test of a 6-dof parallel platform with dense ball shafting as a revolute joint," *Appl Sci* **11**(14), 6268 (2021).
[10] Y. Yu, Z.-B. Xu, Q.-W. Wu, P. Yu, S. He and G.-Q. Wang, "Kinematic analysis and testing of a 6-RR RP RR parallel manipulator," *Proceed Inst Mech Eng, Part C: J Mech Eng Sci* **231**(13), 2515–2527 (2017).
[11] Y. Zhang, H. Han, H. Zhang, Z. Xu, Y. Xiong, K. Han and Y. Li, "Acceleration analysis of 6-RR-RP-RR parallel manipulator with offset hinges by means of a hybrid method," *Mech Mach Theory* **169**, 104661 (2022).
[12] S. Staicu, "Dynamics of the 6-6 Stewart parallel manipulator," *Robot Cim-INT Manuf* **27**(1), 212–220 (2011).
[13] L.-W. Tsai, "Solving the inverse dynamics of a Stewart-Gough manipulator by the principle of virtual work," *J Mech Design* **122**(1), 3–9 (2000).
[14] Y. Zhao and F. Gao, "Inverse dynamics of the 6-dof out-parallel manipulator by means of the principle of virtual work," *Robotica* **27**(2), 259–268 (2009).
[15] F. Asadi and S. H. Sadati, "Full dynamic modeling of the general stewart platform manipulator via Kane's method," *Iranian J Sci Tech, Trans Mech Eng* **42**(2), 161–168 (2018).
[16] J. Enferadi and K. Jafari, "A Kane's based algorithm for closed-form dynamic analysis of a new design of a 3RSS-S spherical parallel manipulator," *Multibody Syst Dyn* **49**(4), 377–394 (2020).
[17] P. Wu, H. Xiong and J. Kong, "Dynamic analysis of 6-SPS parallel mechanism," *Int J Mech Mater Des* **8**(2), 121–128 (2012).

[18] Q. Zhang, J. K. Mills, W. L. Cleghorn, J. Jin and C. Zhao, "Trajectory tracking and vibration suppression of a 3-PRR parallel manipulator with flexible links," *Multibody Syst Dyn* **33**(1), 27–60 (2015).
[19] T. Zhao, M. Geng, Y. Chen, E. Li and J. Yang, "Kinematics and dynamics Hessian matrices of manipulators based on screw theory," *Chin J Mech Eng* **28**(2), 226–235 (2015).
[20] J. Gallardo-Alvarado, C. R. Aguilar-Nájera, L. Casique-Rosas, L. Pérez-González and J. M. Rico-Martínez, "Solving the kinematics and dynamics of a modular spatial hyper-redundant manipulator by means of screw theory," *Multibody Syst Dyn* **20**(4), 307–325 (2008).
[21] J. Gallardo, J. M. Rico, A. Frisoli, D. Checcacci and M. Bergamasco, "Dynamics of parallel manipulators by means of screw theory," *Mech Mach Theory* **38**(11), 1113–1131 (2003).
[22] Z. Geng, L. S. Haynes, J. D. Lee and R. L. Carroll, "On the dynamic model and kinematic analysis of a class of Stewart platforms," *Robot Auton Syst* **9**(4), 237–254 (1992).
[23] J. D. Lee and Z. Geng, "A dynamic model of a flexible stewart platform," *Comput Struct* **48**(3), 367–374 (1993).
[24] Q. Zou, D. Zhang and G. Huang, "Dynamic performance evaluation of the parallel mechanism for a 3T2R hybrid robot," *Mech Mach Theory* **172**, 104794 (2022).
[25] B. Dasgupta and T. S. Mruthyunjaya, "A Newton-Euler formulation for the inverse dynamics of the Stewart platform manipulator," *Mech Mach Theory* **33**(8), 1135–1152 (1998).
[26] J. He, H. Zheng, F. Gao and H. Zhang, "Dynamics and control of a 7-DOF hybrid manipulator for capturing a non-cooperative target in space," *Mech Mach Theory* **140**, 83–103 (2019).
[27] R. F. Abo-Shanab, "Dynamic modeling of parallel manipulators based on Lagrange-D'Alembert formulation and Jacobian/Hessian matrices," *Multibody Syst Dyn* **48**(4), 403–426 (2020).
[28] Y. Ting, Y.-S. Chen and H.-C. Jar, "Modeling and control for a Gough-Stewart platform CNC machine," *J Robotic Syst* **21**(11), 609–623 (2004).
[29] Z. Bingul and O. Karahan, "Real-time trajectory tracking control of Stewart platform using fractional order fuzzy PID controller optimized by particle swarm algorithm," *Indust Rob: The Inter J Rob Res App* **49**(4), 708–725 (2021).
[30] H. Cheng, Y.-K. Yiu and Z. Li, "Dynamics and control of redundantly actuated parallel manipulators," *IEEE/ASME Trans Mech* **8**(4), 483–491 (2003).
[31] H. Pang and M. Shahinpoor, "Inverse dynamics of a parallel manipulator," *J Robotic Syst* **11**(8), 693–702 (1994).
[32] W. M. Silver, "On the equivalence of Lagrangian and Newton-Euler dynamics for manipulators," *Int J Rob Res* **1**(2), 60–70 (1982).
[33] Z. Chen and X. Wang, "Dynamic modeling and residual vibration suppression of the redundantly-actuated cable driving parallel manipulator," *IEEE Access* **8**, 99422–99430 (2020).
[34] A. Arian, B. Danaei, H. Abdi and S. Nahavandi, "Kinematic and dynamic analysis of the Gantry-Tau, a 3-DoF translational parallel manipulator," *Appl Math Model* **51**, 217–231 (2017).
[35] J. He, H. Zheng, F. Gao and H. Zhang, "Dynamics and control of a 7-DOF hybrid manipulator for capturing a non-cooperative target in space," *Mech Mach Theory* **140**, 83–103 (2019).
[36] Y. Saad and M. H. Schultz, "GMRES: A generalized minimal residual algorithm for solving nonsymmetric linear systems," *Siam J Sci Stat Comp* **7**(3), 856–869 (1986).

Appendix
Details of the inverse kinematic

The reference frame transformation relation for the *j*th leg is as follows:

$$\mathbf{T}_{leg} = \mathbf{T}_1 \cdot \mathbf{T}_2 \cdot \mathbf{T}_3 \cdot \mathbf{T}_4 \cdot \mathbf{T}_5 \cdot \mathbf{T}_6 \tag{29}$$

Because the frames $\mathcal{P}_j$ and $\mathcal{B}_j$ are known in frames $\mathcal{P}$ and $\mathcal{B}$, when the position of the MP is determined, the equivalent reference frame transformation relation for the *j*th leg is also obtained. The homogeneous transformation matrix of its frame system $\mathbf{T}'_{leg}$ is given by:

$$\mathbf{T}'_{leg} = \mathbf{T}_{\mathcal{B}_j}^{-1} \cdot \mathbf{T}_{\mathcal{P}} \cdot {}^{\mathcal{P}}\mathbf{T}_{\mathcal{P}_j} \tag{30}$$

where $\mathbf{T}_{\mathcal{B}_j}$ represents the transformation matrix of $\mathcal{B}_j$ concerning the frame $\mathcal{B}$, $\mathbf{T}_{\mathcal{P}}$ represents the transformation matrix of the frame $\mathcal{P}$ concerning the frame $\mathcal{B}$, and ${}^{\mathcal{P}}\mathbf{T}_{\mathcal{P}_j}$ represents the transformation matrix of the frames $\mathcal{P}_j$ concerning the frame $\mathcal{P}$.

As demonstrated by the equivalence relation, Eq. (29) is equivalent to Eq. (30):

$$\mathbf{T}_{leg} - \mathbf{T}'_{leg} = \mathbf{Q} = 0 \tag{31}$$

At this point, we have the equivalent relation matrix for one leg. Equation (31) contains all six unknowns of $\mathbf{q}_{ij}$. Each element can be considered as a separate equation, so the six matrix elements

can be selected to form the following nonlinear system of equations:

$$\boldsymbol{\Phi}_j = \begin{cases} \Phi_1\left(\mathbf{q}_{ij}^{\mathrm{T}}\right) = \mathbf{Q}\,(1,2) = 0 \\ \Phi_2\left(\mathbf{q}_{ij}^{\mathrm{T}}\right) = \mathbf{Q}\,(1,3) = 0 \\ \Phi_3\left(\mathbf{q}_{ij}^{\mathrm{T}}\right) = \mathbf{Q}\,(1,4) = 0 \\ \Phi_4\left(\mathbf{q}_{ij}^{\mathrm{T}}\right) = \mathbf{Q}\,(2,1) = 0 \\ \Phi_5\left(\mathbf{q}_{ij}^{\mathrm{T}}\right) = \mathbf{Q}\,(2,2) = 0 \\ \Phi_6\left(\mathbf{q}_{ij}^{\mathrm{T}}\right) = \mathbf{Q}\,(3,1) = 0 \end{cases} \tag{32}$$

Each of these equations is nonlinear and contains several variables. Thus, the solution can only be obtained indirectly. Therefore, the Newton–Raphson iteration method is applied to solve this nonlinear system for the *j*th leg:

$$\left[\mathbf{q}_{ij}\right]_{(k+1)} = \left[\mathbf{q}_{ij}\right]_{(k)} - \left[\frac{\partial \boldsymbol{\Phi}_j}{\partial \mathbf{q}_{ij}}\right]_{(k)}^{-1} \cdot \left[\mathbf{q}_{ij}\right]_{(k)} \tag{33}$$

Cite this article: H. Huang, H. Han, D. Li, Z. Xu and Q. Wu (2024). "Inverse dynamics analysis of a 6-RR-RP-RR parallel manipulator with offset universal joints", Robotica **42**, 1549–1567. https://doi.org/10.1017/S0263574724000365